Pertanika J. Sci. & Technol. 34 (S3): 71 - 100 (2026)

PERTANIKA JOURNALS

SCIENCE & TECHNOLOGY

Journal homepage: http://www.pertanika.upm.edu.my/

Deep Learning and Signal Processing Synergy: Multitask Deep Neural Networks (MLT-DNNs) and Second-Order Blind Identification (SOBI) for Cybersickness Detection

Bisani Leela Padmavathi[1]* and J. Avanija[2]

[1]Department of Computer Science and Engineering, School of Computing, Mohan Babu University, Sree Sainath Nagar, 517102 Tirupati, Andhra Pradesh, India
[2]Department of Artificial Intelligence and Machine Learning, School of Computing, Mohan Babu University, Sree Sainath Nagar, 517102 Tirupati, Andhra Pradesh, India

ABSTRACT

Cybersickness in virtual reality (VR) environments presents an important challenge for user experience. Accurate evaluation approaches are essential for mitigating or preventing cybersickness among users. Compared to traditional subjective user studies, such as forms, electroencephalography (EEG) offers the advantage of high temporal resolution, enabling more precise real-time evaluation. EEG signals offer a promising avenue for objective detection of cybersickness, as they capture real-time neural responses. This study introduces a novel framework that combines Multitask Deep Neural Networks (MLT-DNNs) with Second-Order Blind Identification (SOBI) to enhance the accuracy and robustness of cybersickness detection. The MLT-DNN architecture leverages multitask learning to simultaneously predict cybersickness severity and related physiological states, such as stress and cognitive load, thereby enabling a comprehensive understanding of user experiences. SOBI is employed to pre-process EEG signals by separating and denoising independent source components, effectively reducing artefacts and noise. This integration of SOBI with MLT-DNN ensures high-quality input features, improving classification performance. The proposed framework is validated using a benchmark EEG dataset collected from VR users exposed to varying cybersickness-inducing scenarios. Experimental results demonstrate superior performance over baseline models, with significantly higher detection accuracy and reduced computational overhead. By combining advanced signal processing and deep learning methodologies, this work provides a scalable solution for real-time cybersickness monitoring

ARTICLE INFO

Article history:
Received: 03 August 2026
Accepted: 29 September 2026
Published: 20 November 2026

DOI: https://doi.org/10.47836/pjst.34.S3.04

E-mail addresses:
leelaashwin.b@gmail.com (Bisani Leela Padmavathi)
avans75@yahoo.co.in (J. Avanija)
* Corresponding author

e-ISSN: 2231-8526

© Universiti Putra Malaysia Press

in VR environments, contributing to the development of user-centric VR systems. Furthermore, this approach underscores the potential of multitask learning in addressing complex neurophysiological phenomena in human-computer interaction.

Keywords: Cybersickness, EEG, machine learning, multitask deep neural network, second-order blind identification, signal processing, virtual reality

INTRODUCTION

A wide range of businesses, including education, healthcare, and entertainment, have embraced VR. However, a major obstacle to its safe adoption is cybersickness, which is often associated with VR use. When people use virtual reality technology to immerse themselves in a virtual environment, they may experience cybersickness, a form of motion sickness (Chang et al., 2023). This condition results from perceived visual motion and the amount of detected vestibular motion; it is characterised by nausea, oculomotor pain, and disorientation. Some effects of using VR include dizziness, loss of balance, and impaired coordination. Cybersickness affects 50-80% of viewers of virtual reality content. Eradication of cybersickness is crucial to the growth of virtual reality. Thus, it is necessary to determine the extent of cybersickness associated with VR content to properly control it during its creation (Caserman et al., 2021).

The most frequently used assessment methods in the past were questionnaires and other subjective measures. As a word of caution, questionnaire-based methods rely on participants' perceptions and therefore can be sensitive to variation among participants (Martin et al., 2020). Furthermore, because these evaluations are usually conducted post-trial, data collection relies solely on retrospective measurements, which makes continuous monitoring of cybersickness challenging. The temporal lobe is involved in vestibular function, and the occipital lobe is involved in vision. The human brain is the primary organ of the central nervous system (Krokos & Varshney, 2022). When studying the physiological correlates of cybersickness, brain data are closely linked to the phenomenon. Previous studies have found a high level of dependency of participants' cybersickness in immersive virtual environments and EEG frequency characteristics. Moreover, because EEG is continuous and offers high temporal resolution, cybersickness can be evaluated automatically and continuously using EEG-based assessment methods. Consequently, cybersickness can be quantified and assessed with high reliability and practicability using EEG-based approaches (Heo & Yoon, 2020).

There are many VR devices available for creating an interesting experience. Among consumer VR systems, VR head-mounted displays (HMDs) are the most widely used. HMDs feature two screens positioned in front of the user's eyes. To represent each eye's perspective, digital images are presented in the appropriate perspective on each screen (Ahir et al., 2020).

A shell housing the screens and sensors continuously monitors the user's head movements and adjusts the virtual environment accordingly. Information obtained through the senses forms the basis of awareness of one's immediate surroundings. VR HMDs must replace real sensory experiences with computer-generated ones so that users can actively perceive them using their typical sensorimotor dependencies. The term "being" is used to describe the illusion of existing within a virtual environment. VR HMDs enable users to experience virtual surroundings as real by providing a wide field of view, stereoscopic vision, and real-time sensory updates (Porcino et al., 2020). This sense of presence leads people to behave realistically within virtual reality. With their compact size, lightweight design, and expanded field of view, HMDs enhance immersion in virtual environments by offering a variety of interactive experiences. The newest generation of HMDs enables users to "look around," "turn around," and engage realistically in a virtual environment by simulating changes in visual display as the head and torso are tilted. The latest generation of HMDs can generally be described as highly immersive and subjective (Teixeira & Palmisano, 2021).

Research on Our Work

The present research concerns the integration of deep learning with signal processing techniques to improve the recognition of cybersickness. Therefore, in this paper, we propose using a signal processing technique called SOBI in conjunction with a newly introduced multitask DNN to process physiological signals, including EEGs. This integration enhances the identification of cybersickness by incorporating the classification features of the multitask DNNs with the feature extraction features of the SOBI. The results of this work show how deep learning and modern signal processing techniques can be applied to address several issues in the analysis of physiological signals.

Motivation of This Research

This work is inspired by the growing application of virtual and augmented reality (VR/AR) technologies, which, although they hold transformative promise, can cause cybersickness that hinders their adoption. Existing approaches to detecting such behaviour are inaccurate and not applicable in real time. This study will seek to fill this gap using deep learning and signal processing – multitask DNNs and Second-Order Blind Identification (SOBI) for enhancing cybersickness detection. In this way, the study aims to create a new, effective, and practical system by integrating these approaches to improve VR/AR usability and detect cybersickness.

Main Contribution of Our Work

- To enhance the precision and resilience of cybersickness detection, this study introduces a novel framework that integrates SOBI with MLT-DNNs.

- The MLT-DNN architecture uses multitask learning to estimate cybersickness intensity and other correlated physiological conditions like stress and cognitive workload, which will enhance the understanding of cybersickness.
- Experimental results highlight superior performance compared to baseline models, demonstrating a significant increase in detection accuracy and reduced computational overhead.
- This work proposes a real-time cybersickness detection framework that integrates signal processing and deep learning to create user-oriented VR systems.

Paper Organisation

Figure 1 displays the organisation of the paper.

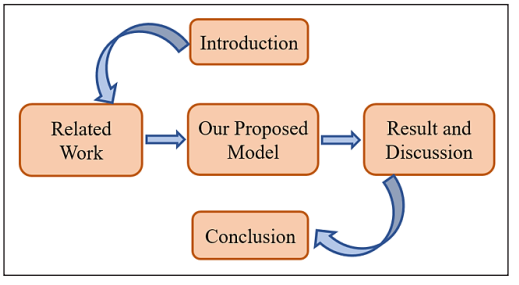

Figure 1. Organisation of the research

Related Work

Cybersickness, a condition characterised by discomfort, nausea, dizziness, and other physiological symptoms, often arises during interactions with virtual or augmented reality environments. As these technologies become more integrated into our daily lives, ranging from gaming and education to healthcare and professional training, understanding and addressing cybersickness is essential to ensure user comfort and widespread adoption. This survey aims to explore perceptions, experiences, and potential indicators of cybersickness to enhance detection and mitigation strategies.

Kourtesis et al. (2024) examined the background of cybersickness and its relationship to cognitive and motor performance. The CSQ-VR and the MSSQ were completed by 30 participants, aged between 20 and 45 years, during the VR roller coaster. In addition to the cognitive and psychomotor activities during the VR session, the participants were administered the CSQ-VR before and after the ride. It was found that the most important factors influencing adult cybersickness were susceptibility to motion sickness and pupil size.

Papaefthymiou et al. (2024) studied the effects of immersion, task execution, and subject characteristics on cybersickness symptoms across various stages of VR exposure. To this end, 47 subjects aged between 18 years and 45 years completed the Deary–Liewald Reaction Time (DLRT) task and the Cybersickness in Virtual Reality Questionnaire (CSQ-VR). Symptoms of cybersickness were assessed at four stages: participants' responses to questionnaires completed before and after the 12-minute rollercoaster ride (programmed to induce cybersickness) and before and after VR immersion. The results showed that

subjects' motion sickness symptoms worsened after the rollercoaster ride but were partially alleviated during the post-ride tasks.

Martirosov et al. (2022) conducted an experiment to examine the correlation between immersion and cyber illness among participants. Ninety participants, aged 19-36, were divided into two groups, with participants in the first group having higher levels of virtual reality exposure than those in the second group. The low-immersive group used monocular, screen-based PCs; the semi-immersive group used a CAVE with stereoscopic projectors; the highly immersive group used VR head-mounted displays; and the control group received no immersion.

According to Zaidi et al. (2023), to predict outcomes in computer science, the following ML and AI methods should be employed: SVM, DT, and KNN. Our findings revealed that DT and SVM achieve higher test accuracy than KNN, and DT achieves higher training accuracy than both SVM and KNN. When using machine learning to develop better solutions to computer science challenges, developers can anticipate potential problems when designing VR projects.

The issue of indirectly identifying and quantifying cybersickness in virtual reality based on physiological signals is discussed by Sameri et al. (2024). As a result, they propose a multimodal strategy that combines self-reported measurements with physiological data. Our experimental paradigm involves a roller coaster simulation and employs a mixed-methods approach integrating quantitative and qualitative analyses. By utilising statistical analysis and machine learning techniques, the study examines physiological data collected from 22 participants who were exposed to a virtual-reality roller coaster experience.

The systematic review by Yang et al. (2022) focuses on 26 selected studies on the automatic detection of cybersickness using machine learning applied to biometric and neurophysiological signals collected via wearable technology. The review examines techniques, data processing methods, machine learning architectures, and recommendations for further research on cybersickness prediction and detection. Various machine learning architectures, features, participant activities, and immersion environments were identified. Despite advancements in cybersickness detection methods, there is currently no model in the literature capable of predicting first-instance incidents.

The authors (Qu et al., 2022) used physiological sensors to monitor cybersickness in real time, collect data, and apply a deep learning model to quantify the elements contributing to cybersickness. Additionally, they developed a passive navigation task and a VR experimental platform designed to induce cybersickness in users. In the experiment, to train the LSTM Attention neural network model, the position and rotation of the user's virtual figure's bone, as well as physiological signals such as electrodermal activity (EDA) and electrocardiogram (ECG), were captured in real time.

Research Gap

While there has been significant progress in VR technology, the precise and timely identification of cybersickness remains a major challenge. Current approaches can be based on self-estimations, which are notoriously unreliable, or rely on physiological data, which are not suitable for real-time monitoring and diffusion. Furthermore, the interaction between content-specific subcomponents, such as motion patterns and latency, and user-specific factors, such as age, gender, and prior VR exposure, remains poorly understood, leading to variable detection performance. This highlights the importance of robust, accurate, and versatile detection systems that integrate data from multiple sensors with state-of-the-art machine learning techniques to improve predictive accuracy and practicality across various VR applications.

Problem Identification of the Existing System

- Existing systems often fail to provide precise, real-time detection of cybersickness symptoms, limiting their usability in dynamic virtual environments.
- Many systems rely on generalised models that do not account for individual variability in susceptibility to cybersickness, leading to inconsistent results.
- Current detection methods primarily depend on a single source of data, such as physiological signals or user behaviour, without integrating multiple modalities for a more comprehensive analysis.
- Numerous solutions require users to wear bulky or intrusive sensors, which can exacerbate discomfort and reduce user acceptance.

Proposed Model

The study presents a new approach of combining SOBI and MLT-DNNs to improve the performance and reliability of cybersickness detection. The MLT-DNN architecture uses multitask learning to estimate cybersickness intensity and related physiological states, including stress and cognitive load, thereby providing a holistic view of the user experience. In this paper, SOBI is used to preprocess EEG signals through independent source separation and filtering out artefacts and noise. The integration of SOBI and MLT-DNN guarantees high-quality input features, thereby enhancing classification. The applicability of the proposed framework is demonstrated using a benchmark EEG dataset acquired from VR users experiencing different cybersickness-eliciting conditions. The model diagram is illustrated in Figure 2.

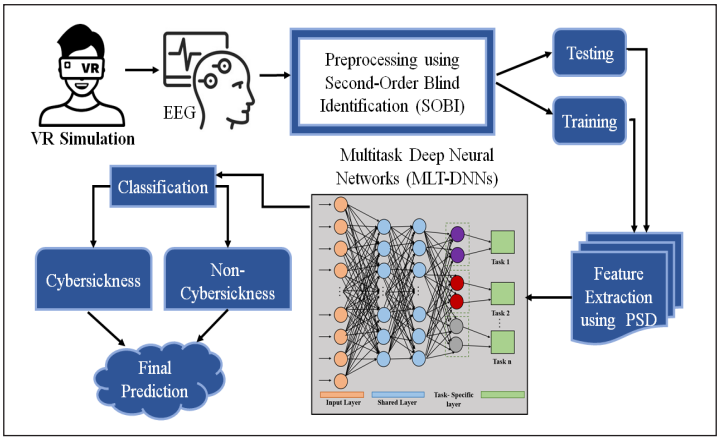

Figure 2. Block diagram of the proposed model

Dataset

The dataset is a collection of user feedback obtained in VR settings, specifically user choices, mood, and physiological characteristics such as heart rate variability and skin conductance (Joshi, 2023). The main goal of this study is to contribute to the development of VR technologies by focusing on users' experiences, with particular attention to enhancing VR design, user protection, and personalisation. By analysing the physical and emotional reactions to different VR situations, the dataset helps developers design appropriate and engaging VR experiences for people. The main variables in the dataset are Age (the participant's age during the VR session), Gender (the participant's gender), and User ID (the participant's identification number). Other variables, such as the VR Headset Type, the duration the respondent spent with the VR, and the Motion Sickness Rating, also give information about the VR equipment and the respondent. The dependent variable in this study is Immersion Level, which measures the extent to which users felt immersed while using the mobile application, on a 1-5 Likert scale. This dataset will be useful to developers for improving VR systems, increasing user satisfaction and immersion, and designing VR for various clients.

Signal Pre-Processing

This makes signal preprocessing important for improving data quality and for extracting useful features for identifying cybersickness. This process involves three key steps: noise removal, normalisation, and Second Order Blind Identification (SOBI) (Liu et al., 2019). These steps help ensure that the signals are clean and free of interference and can be used to decompose independent components associated with cybersickness.

Noise Removal

Signal filtering is used to eliminate many unwanted noise and artefacts present in the signal. To remove baseline drifts at low frequencies and high-frequency noise, a band-pass filter is employed. The filtered signal $y(t)$ is computed using the convolution of the raw signal $x(t)$ with the filter impulse response $h(t)$ as in Equation 1:

$$y(t) = \int_{-\infty}^{\infty} x(\tau) \quad h(t-\tau)d\tau \qquad [1]$$

For physiological signals such as EEG, the normal frequency is between 0.5Hz and 50Hz as in Equation 2.

$$h(t) = A[\sin(2\pi f_{high}t) - \sin(2\pi f_{low}\, t)] \qquad [2]$$

Where f_{low} and f_{high} signify the lower and upper cutoff frequencies, correspondingly.

Additionally, baseline drift can be removed using a moving average filter, which subtracts the local average over a window N as in Equation 3:

$$y(t) = x(t) - \frac{1}{N}\sum_{i=t-N/2}^{t+N/2} x(i) \qquad [3]$$

This helps in making the signals free from long-term trends and high-frequency noise.

Standardisation

To ensure consistency across participants and sessions, the signals are normalised. Each signal value x is transformed into a standardised value z using Equation 4:

$$z = \frac{x-\mu}{\sigma} \qquad [4]$$

Here, μ is the mean of the signal, and σ is the standard deviation. This makes it possible to eliminate individual variability and hence improve the accuracy of the analysis by reducing it to a standard form with a mean of zero and variance of one.

Second-Order Blind Identification (SOBI)

SOBI is an enhanced signal processing method used to extract independent components from observed signals. It starts by computing the covariance matrix of the observed signal vector $x(t)$ at different time lags τ as in Equation 5:

$$C_x(\tau) = \mathbb{E}[x(t)x^T(t+\tau)] \qquad [5]$$

Here, $C_x(\tau)$ captures the relationships between signal channels at a time lag τ. SOBI performs joint diagonalisation of these covariance matrices to estimate a transformation matrix W that minimises off-diagonal elements as mentioned in Equation 6:

$$WC_x(\tau)W^T\Lambda(\tau) \quad [6]$$

Where $\Lambda(\tau)$ is a diagonal matrix representing independent signal components.

The independent components $s(t)$ are then computed as specified in Equation 7:

$$s(t) = W_x(t) \quad [7]$$

These components are then compared to determine which are most associated with cybersickness symptoms, such as EEG patterns associated with motion sickness or cognitive load.

Feature Extraction Using Power Spectral Density (PSD)

In all the feature extraction methodologies for physiological signals, especially the EEG, PSD is among the most efficient (Alam et al., 2021). PSD is a quantitative measure of how a signal's power is distributed across its frequencies and is used to identify frequency-specific patterns of cybersickness. PSD can determine the physiological and cognitive conditions that lead to cybersickness symptomatology by employing the delta, theta, alpha, and beta bands.

To compute the PSD, the signal's autocorrelation function $R_{xx}(\tau)$ is analysed in the frequency domain using the Fourier Transform as mentioned in Equation 8:

$$PSD(f) = \int_{-\infty}^{\infty} R_{xx}(\tau)e^{-j2\pi fr}\,d\tau \quad [8]$$

Here, $R_{xx}(\tau) = \mathbb{E}\lfloor x(t)x(t+\tau)\rfloor$ is the autocorrelation function of the signal $x(t)$, which represents how the signal correlates with itself at different time lags τ, and f is the frequency. For discrete signals, PSD can be efficiently estimated using the Fast Fourier Transform (FFT):

Where N is the length of the signal, $X(f_k)$ is the Fourier Transform of the signal at frequency f_k.

The power within specific frequency bands, such as delta (0.5–4 Hz), theta (4–8 Hz), alpha (8–13 Hz), and beta (13–30 Hz), can be computed using the PSD. These bands provide meaningful insights, such as elevated theta power reflecting cognitive stress or altered alpha power indicating discomfort.

To standardise the characteristics for model input, the relative power of each frequency band is computed as in Equation 9:

$$P_{relative} = \frac{\int_{f_{low}}^{f_{high}} PSD(f)df}{\int_{f_{min}}^{f_{max}} PSD(f)df} \quad [9]$$

Here f_{low} and f_{high} is the boundaries of the specific frequency band, f_{min} and f_{max} is the full frequency range of the signal.

By converting raw physiological signals into PSD features, the model can extract more frequency-domain information, which helps it identify patterns associated with cybersickness. These features are very useful for the severity levels and the early signs of the disease.

Multitask Deep Neural Networks (MLT-DNNs)

Advanced machine learning architectures, known as MLT-DNN, are designed to handle multiple related tasks simultaneously by leveraging shared representations to enhance performance across all tasks (Chang et al., 2024). These models operate on the principle of joint learning, wherein shared parameters W are trained to optimise multiple loss functions L_t corresponding to each task t. The objective function of an MLT-DNN can be expressed as in Equation 10:

$$\min_{W,\{W_t\}} \sum_{t=1}^{T} \lambda_t L_t(W, W_t) \quad [10]$$

Where T is the number of tasks, W_t are task-specific parameters, and λ_t The weights control the importance of each task. The shared parameters W enable the model to capture common features across tasks, improving generalisation and reducing overfitting compared to training separate models in Figure 3 shows the MLT-DNN model.

A standard MLT-DNN consists of shared layers followed by task-specific layers. Let h_s represent the output of the shared

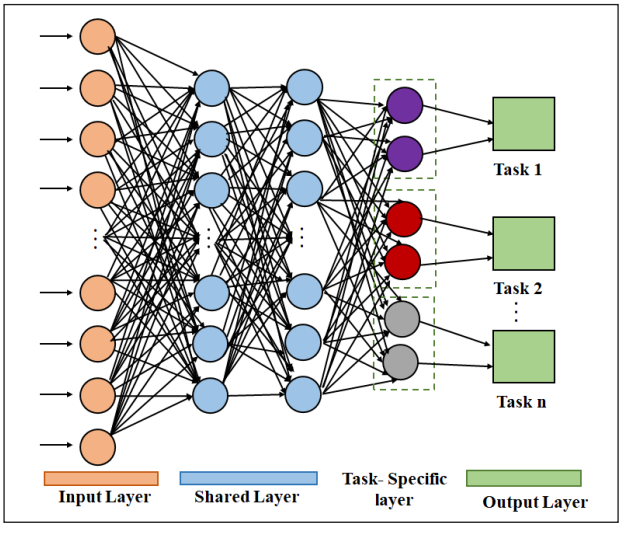

Figure 3. The architecture of the MLT-DNN model

layers and $h_{t,i}$ the output for the i-th input of the task t. This can be expressed as in Equations 11 and 12:

$$h_s = f_s(x; W_s) \quad [11]$$

$$h_{t,i} = f_t(h_s; W_t) \quad [12]$$

Here, W_s and W_t are the weights of the shared and task-specific layers, respectively. During backpropagation, gradients from all tasks contribute to updating the shared parameters W_s as in Equation 13:

$$\frac{\partial L}{\partial W_s} = \sum_{t=1}^{T} \lambda_t \frac{\partial L_t}{\partial W_s} \quad [13]$$

Another advantage of the MLT-DNNs is that they enable the sharing of data distributions across tasks to overcome data scarcity in individual tasks. For instance, in a multitasking environment with tasks A and B, the model can leverage task dependencies. If $g(x)$ represents a shared latent feature, then predictions for tasks can be given by Equations 14 and 15:

$$yA = g(x)W_A \quad [14]$$

$$yA = g(x)W_B \quad [15]$$

Regularisation is crucial in MLT-DNNs to prevent the overfitting of shared parameters to a single task at the expense of others. Common approaches include l_2-regularisation and dropout as in Equation 16:

$$R(W_s) = \frac{\lambda}{2}||W_s||^2 \quad [16]$$

The design of loss functions and weighting factors λ_t significantly impacts multitasking performance. A dynamic weighting scheme can be employed to balance losses as mentioned in Equation 17:

$$\lambda_t = \frac{exp\,(-L_t)}{\sum_{k=1}^{T} exp\,(-L_k)} \quad [17]$$

The cross-stitch units are also a new concept that allows certain features to be selectively shared between tasks. If z^A and z^B represent task-specific features, cross-stitching is defined as specified in Equations 18 and 19:

$$z^{A'} = \alpha z^A + \beta z^B \quad [18]$$

$$z^{B'} = \gamma z^A + \delta z^B \quad [19]$$

In MLT-DNNs, $\alpha, \beta, \gamma, \delta$, these are learned parameters used in cross-stitch units to control the degree of feature sharing between tasks. These parameters control the relative weighting of task-specific and general features to accommodate task dependencies while preserving task-specific differentiation.

Some of the fields where MLT-DNNs are applied include NLP, which involves tasks such as POS tagging and syntactic parsing that require similar representations. For instance, in NLP, word embeddings (E) used across different tasks can be trained together as mentioned in Equation 20:

$$E' = E - \eta \frac{\partial L}{\partial E} \quad [20]$$

Finally, the optimisations in MLT-DNNs include gradient clipping and adaptive learning rates, with optimisers such as Adam or RMSProp as specified in Equation 21.

$$\Delta W = \frac{\eta}{\sqrt{v_t + \epsilon}} m_t \quad [21]$$

In the context of optimisation algorithms like Adam, m_t and v_t represent the first and second moment estimates of the gradients, respectively. m_t is the exponentially weighted moving average of the gradients, capturing the mean, while v_t tracks the variance by computing the moving average of squared gradients. These estimates help control the learning rate and enable stable convergence. The integration of shared representation, dynamic task weighting, and regularisation strategies makes MLT-DNNs a reliable model for effectively solving complex multitask problems.

Advantages of the Proposed Model

- Combines the strengths of multitask DNN and SOBI to enhance detection performance.
- Combines deep learning's ability to extract nonlinear characteristics with SOBI's skill in isolating and processing signal parts.

- Simultaneously addresses multiple related tasks, such as classification and regression, for a comprehensive cybersickness assessment.
- Efficiently processes complex, multi-channel signal data, ensuring adaptability to diverse real-world scenarios.

RESULT AND DISCUSSIONS

Experimental Setup

To train the network, we applied the Adam optimiser with a learning rate of 0.001. The experiment was performed on a server system with an Intel i9-10900X CPU, 128 GB of RAM and Nvidia RTX 3090 GPU.

Performance Metrics

Root Mean Square Error (RMSE)

RMSE, which calculates the difference between expected values $(\hat{y}_i)$ and actual values (y_i). It is a widely used statistic for assessing a model's accuracy. Better model performance is indicated by a lower RMSE, which measures the average magnitude of prediction errors as in Equation 22:

$$RMSE = \sqrt{\frac{1}{n}\sum_{i=1}^{n}(\hat{y}_i - y_i)^2} \quad [22]$$

Pearson's Linear Correlation Coefficient (PLCC)

It measures the linear relationship between two variables and assesses both its direction and strength. A complete negative correlation is represented by a value of -1, a perfect positive correlation by a value of 1, and no correlation by a value of 0. In regression tasks, PLCC is frequently used to evaluate the consistency between expected and actual data, as in Equation 23:

$$PLCC = \frac{\sum_{i=1}^{n}(x_i-\bar{x})(y_i-\bar{y})}{\sqrt{\sum_{i=1}^{n}(x_i-\bar{x})^2 \sum_{i=1}^{n}(y_i-\bar{y})^2}} \quad [23]$$

Spearman Rank Order Correlation Coefficient (SROCC)

A monotonic relationship between two ranked variables is measured by the SROCC, which also indicates the direction of the relationship. This test evaluates whether a monotonic

function can adequately characterise the relationship between two datasets and is non-parametric. To calculate the SROCC, use Equation 24:

$$\rho = 1 - \frac{6\sum d_i^2}{n(n^2-1)} \quad [24]$$

Accuracy

One popular metric for assessing a classification model's performance is accuracy. This is the percentage of total instances that are correctly classified. The formula for accuracy is specified in Equation 25:

$$Accuracy = \frac{TP+TN}{TP+TN+FP+FN} \quad [25]$$

F1-Score

The F1-Score is a performance measure that incorporates both precision and recall in problems of classification. It is particularly useful in handling an imbalanced dataset. The F1-Score is an average measure defined as the harmonic mean of precision (P) and recall (R) as in Equation 26.

$$F1 - Score = 2 \times \frac{Pr\ ecision\ \times Re\ call}{Pr\ ecision\ + Re\ call} \quad [26]$$

Processing Time

The total time required to complete a particular computation or process. It is used to assess the efficiency of algorithms in different areas, such as artificial neural networks and signal processing. Processing time can be expressed as in Equation 27:

$$T_{Proces\ sin\ g} = T_{Comp} + T_{IO} \quad [27]$$

Recall

In classification problems, recall measures the percentage of actual positive samples the model recognises. It indicates the extent to which the model can identify positive cases as specified in Equation 28:

$$Re\ c\ all = \frac{TP}{TP+FN} \quad [28]$$

Precision

Precision measures the number of correctly classified positives among all positives predicted by the model in classification problems as mentioned in Equation 29. In this

case, it is especially beneficial to measure the precision of positive predictions when the cost of false positives is high.

$$Pr\,e\,cision = \frac{TP}{TP + FP} \quad [29]$$

Comparative Methods

- **3D-CNN (Three-Dimensional (3D) - Convolutional Neural Network (CNN)) (Lee et al., 2019):** This is accomplished by using disparity, saliency, and optical flow maps from an input video as the inputs for the 3D CNN, representing depth, velocity, and eye movement, respectively.
- **SVM+TDA (Support Vector Machine + Topological Data Analysis) (Hadadi et al., 2022):** When compared to various feature descriptor combinations for physiological time series, the TDA + SVM combination performs statistically similarly to or better than, or matches, more complex and harder-to-interpret approaches.
- **LSTM-Attention (Long Short-Term Memory-Attention) (Qu et al., 2022):** We collected real-time physiological data from participants throughout the experiment, including their skin electrical activity (EDA) and electrocardiogram (ECG), as well as location and bone-rotation data for their virtual avatar, to train the LSTM Attention neural network model.

Table 1 and Figure 4 provide a comprehensive comparison of the F1-score and accuracy across different models: 3D-CNN, SVM+TDA, LSTM-Attention, and the Proposed Framework, evaluated on multiple subjects. The Proposed Framework consistently outperforms the other models, achieving the highest average F1-score (88.03%) and accuracy (97.16%). This marked improvement underscores the success of combining multitask learning with preprocessing techniques for identifying cybersickness. These results show that the Proposed Framework is reliable and extensible in practice, which establishes a new standard for identifying cybersickness.

Table 1
Comparison of F1-score and accuracy analysis with existing systems

Subject	3D-CNN		SVM+TDA		LSTM-Attention		Proposed	
	F1-Score	Accuracy	F1-Score	Accuracy	F1-Score	Accuracy	F1-Score	Accuracy
S1	65.35	65.91	70.91	68.89	62.67	76.56	89.34	94.35
S2	61.22	68.54	79.44	76.45	65.98	70.77	81.44	95.98
S3	76.34	76.34	67.23	71.99	75.98	66.71	90.23	97.77
S4	79.91	76.76	61.55	75.34	76.18	60.91	88.18	98.81
S5	77.44	77.34	69.98	72.26	79.91	79.99	90.99	98.91
Average	72.05	72.97	69.82	72.98	72.14	70.98	88.03	97.16

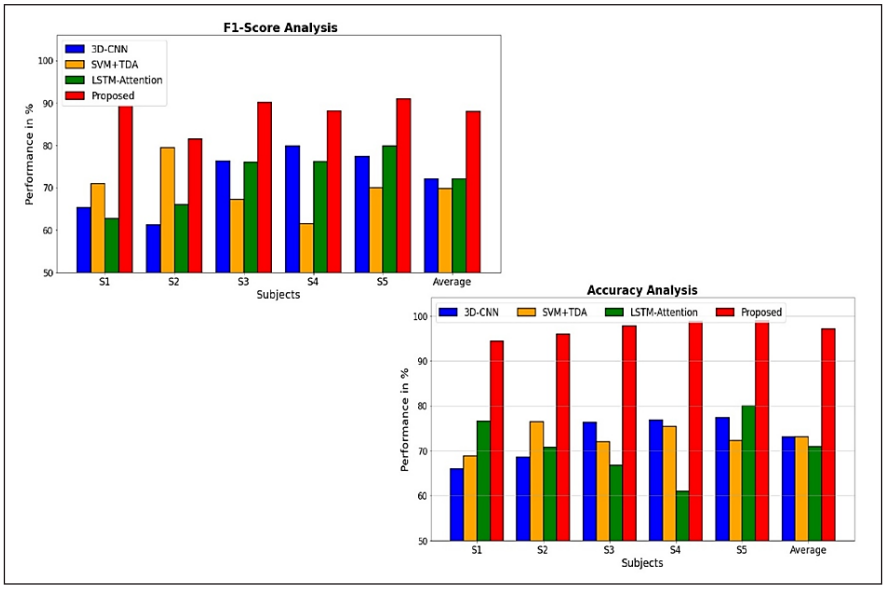

Figure 4. Comparison of F1-score and accuracy analysis with existing systems

Table 2 and Figure 5 highlight the precision and recall performance of various models, including 3D-CNN, SVM+TDA, LSTM-Attention, and the Proposed Framework, across multiple subjects. The Proposed Framework maintains the highest overall average precision (95.97%) and recall (95.92%), while the other approaches are inferior. Such superior performance indicates the high reliability of the Proposed Framework in detecting instances of cybersickness while minimising false negatives. The findings confirm the efficiency of the proposed multitask learning approach and the effectiveness of the more sophisticated preprocessing methods, thereby strengthening its practical applicability to real-world VR scenarios.

Table 2
Comparison of precision and recall analysis with existing systems

Subject	3D-CNN		SVM+TDA		LSTM-Attention		Proposed	
	Precision	Recall	Precision	Recall	Precision	Recall	Precision	Recall
S1	88.45	78.87	76.54	76.91	75.55	75.18	94.65	93.25
S2	80.22	66.19	79.44	78.87	74.14	76.34	95.99	95.55
S3	81.66	60.34	85.44	65.23	76.67	72.18	93.66	97.44
S4	77.65	76.16	80.41	69.91	70.98	76.66	97.66	96.61
S5	70.33	79.44	81.43	69.99	81.33	78.91	97.91	96.78
Average	79.62	72.21	80.65	72.18	75.73	75.85	95.97	95.92

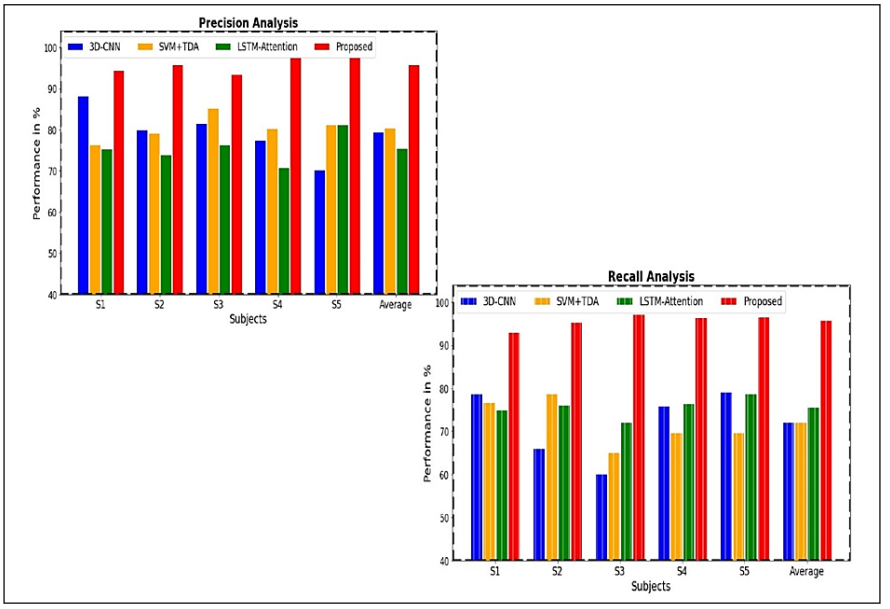

Figure 5. Comparison of precision and recall analysis with existing systems

The PLCC and SROCC are compared across several models, including 3D-CNN, SVM+TDA, LSTM-Attention, and the Proposed Framework, as presented in Table 3 and Figure 6. The Proposed Framework performs best across all experiments, achieving the highest average PLCC of 0.947 and SROCC of 0.952. These results demonstrate its enhanced capacity to sustain high levels of correlation with true cybersickness measures, which in turn suggests reliability and resilience in predictive performance. This supports the Proposed Framework for accurate, scalable assessment of cybersickness in virtual reality settings.

Table 3
Comparison of PLCC and SROCC analysis with existing systems

Subject	3D-CNN		SVM+TDA		LSTM-Attention		Proposed	
	PLCC	SROCC	PLCC	SROCC	PLCC	SROCC	PLCC	SROCC
S1	0.543	0.678	0.765	0.891	0.823	0.611	0.934	0.967
S2	0.765	0.761	0.667	0.875	0.733	0.865	0.913	0.913
S3	0.897	0.789	0.611	0.743	0.776	0.734	0.987	0.954
S4	0.881	0.666	0.788	0.711	0.678	0.771	0.911	0.966
S5	0.880	0.732	0.843	0.764	0.651	0.798	0.904	0.989
Average	0.793	0.725	0.734	0.796	0.730	0.755	0.947	0.952

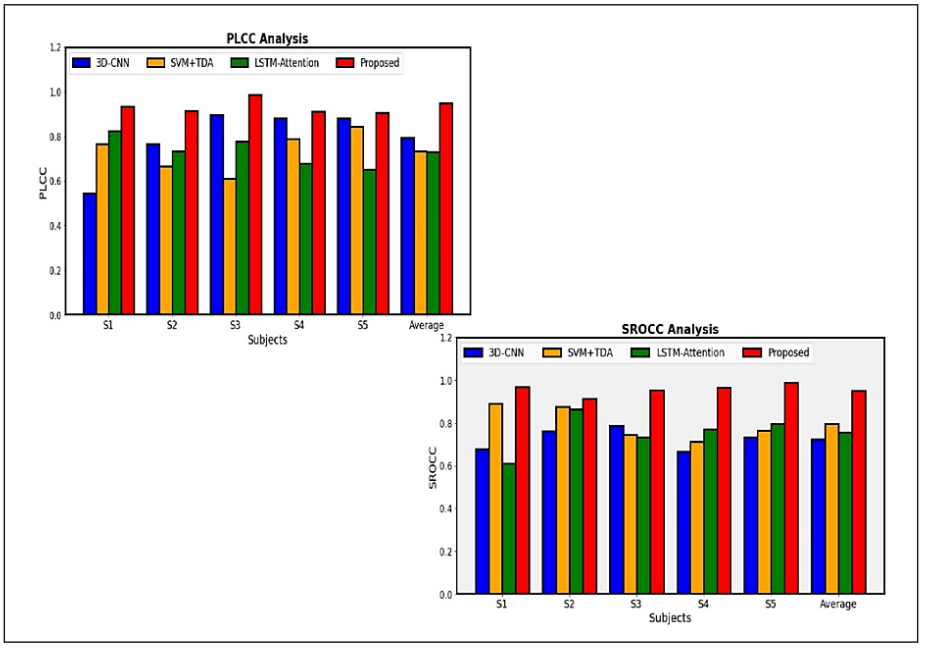

Figure 6. Comparison of PLCC and SROCC analysis with existing systems

Table 4 and Figure 7 show the RMSEs of the 3D-CNN, SVM+TDA, LSTM-Attention, and the Proposed Framework across different subjects. The Proposed Framework also has the lowest RMSE across all subjects, but its overall RMSE of 13.15 is higher than that of the other models. On the other hand, the average RMSE values for the other algorithms, namely SVM+TDA, LSTM-Attention, and 3D-CNN, are 25.85, 34.49, and 37.06, respectively. These results show that the Proposed Framework achieves higher prediction accuracy than the Baseline Model and can minimise prediction errors for cybersickness. This decrease in RMSE indicates the effectiveness of the proposed framework in accurately assessing cybersickness in a real-life VR environment.

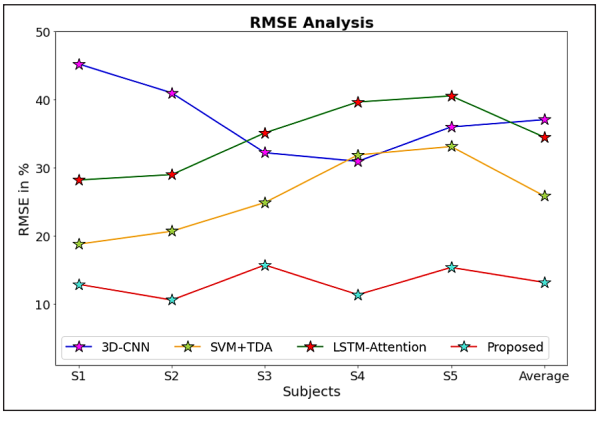

Figure 7. RMSE Analysis for proposed models with existing systems

Table 4
RMSE Analysis for proposed models with existing systems

Subject	3D-CNN	SVM+TDA	LSTM-Attention	Proposed
	RMSE			
S1	45.23	18.76	28.18	12.86
S2	40.98	20.66	28.98	10.55
S3	32.19	24.87	35.11	15.69
S4	30.93	31.87	39.66	11.33
S5	35.98	33.11	40.55	15.33
Average	37.06	25.85	34.49	13.15

Table 5 and Figure 8 present the processing times of the models 3D-CNN, SVM+TDA, LSTM-Attention, and the Proposed Framework for various subjects. The Proposed Framework takes the least time, 4.50ms on average, compared to the other models, which take 17.19ms, 16.26ms, and 10.17ms for 3D-CNN, SVM+TDA, and LSTM-Attention, respectively. This remarkable reduction in processing time underscores the effectiveness of the Proposed Framework, which can be implemented for real-time cybersickness detection in VR environments.

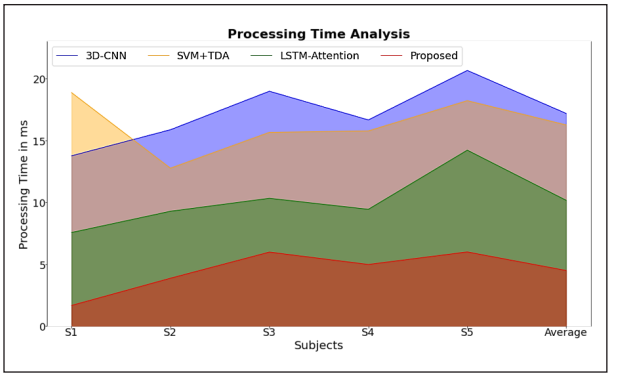

Figure 8. Processing time analysis with existing systems

Table 5
Processing time analysis with existing systems

Subject	3D-CNN	SVM+TDA	LSTM-Attention	Proposed
	Processing Time			
S1	13.765	18.876	7.567	1.675
S2	15.876	12.765	9.286	3.876
S3	18.987	15.664	10.334	5.987
S4	16.667	15.776	9.443	4.987
S5	20.667	18.222	14.223	5.999
Average	17.19	16.26	10.17	4.50

Statistical Analysis

In the next section, the provided dataset provides a strong basis for exploring the application of deep learning and signal processing to counteract cybersickness in VR. It collected 1000 entries reflecting user characteristics, the type of VR headset used, the duration of each session, and users' self-reported levels of cybersickness and immersion, which are beneficial for determining the causes of cybersickness. Factors such as the degree of immersion, the severity of motion sickness, and session duration can indicate critical points that help maintain the necessary level of immersion and reduce discomfort. Moreover, differences in motion sickness across devices indicate where hardware or software improvements can reduce discomfort and enhance VR experiences. The proposed dataset is particularly well-suited to MLT-DNNs and SOBI. While MLT-DNNs can estimate motion sickness intensity and immersion simultaneously from dataset features, SOBI enables signal filtering to extract user-specific factors, such as head movements, that contribute to discomfort. This combination enables more accurate identification of cybersickness, laying the foundation for developing VR systems that adjust their content based on the user's feedback and physiological indicators. The results of this study help to solve not only the problem of cybersickness but also the problem of making VR technologies comfortable for everyone.

Age Distribution Analysis

Table 6 and Figure 9 present users' ages, providing information on the demographic characteristics of VR participants. The data is aggregated by age, with frequencies given across different age brackets. For instance, the dataset shows that the largest user group is between 20 and 30 years old, with a frequency of about 200 users, which means that young people are the main consumers of VR technology. On the other hand, users in the 40 to 50-year age group are relatively few, with approximately 80 users. There are also 50 users under 20, indicating that teenagers are interested in VR technology. However, participation declines among users over 60, with less than 5% of the dataset in this category. Such an age-related trend might be explained by such factors as familiarity with technology, its availability, and a focus on the immersive experience among the younger population. The distribution of the overall data by age shows that

Table 6
The frequency of users across different age groups

S. No.	Age	Frequency
1	18	16
2	19	21
3	20	23
4	21	14
5	22	11
.	.	.
.	.	.
.	.	.
42	26	17
43	27	30

VR is not exclusive to any age group but is more prevalent among the younger generation. These are crucial findings for VR developers to understand their target market, create the right products, and market them accordingly.

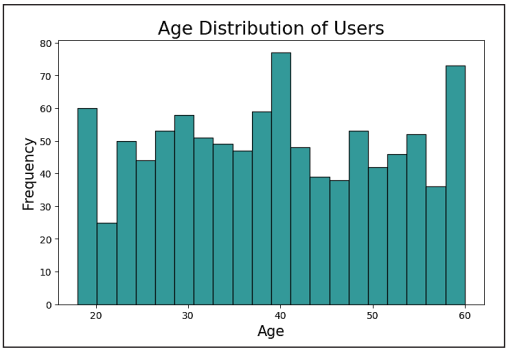

Figure 9. The frequency of users across different age groups

VR Headset Popularity Analysis

Table 7 and Figure 10 present an analysis of VR headset popularity, highlighting user preferences across three primary devices: HTC Vive, Oculus Rift, and PlayStation VR. The distribution of these headsets in the dataset is relatively equal, with Oculus Rift slightly dominating, accounting for 345 respondents. The HTC Vive is second with 336 users, while the PlayStation VR has 325 users. This means there is no single headset with a large user base in virtual reality hardware. The slight edge that Oculus Rift has over its competitors can be attributed to its availability and to certain features that might be more appealing to the masses. The HTC Vive, known for its tracking performance, remains a formidable contender for those seeking a high level of immersion and precision. PlayStation VR is also slightly less popular, but it still has a considerable market share, which can be attributed to the compatibility with PlayStation consoles and relatively low price for the gaming audience. The near-even distribution of these headsets suggests that users have different preferences, which may depend on price, available content, and compatibility. Such findings could help manufacturers and content producers to better understand how to market their products to a broader audience or satisfy specific preferences. More insights into this would be gained if additional information about the users of these headsets were available.

Table 7
The number of users for each VR headset

S. No.	Number of Users	VR Headset
1	Oculus Rift	345
2	HTC Vive	336
3	PlayStation VR	325

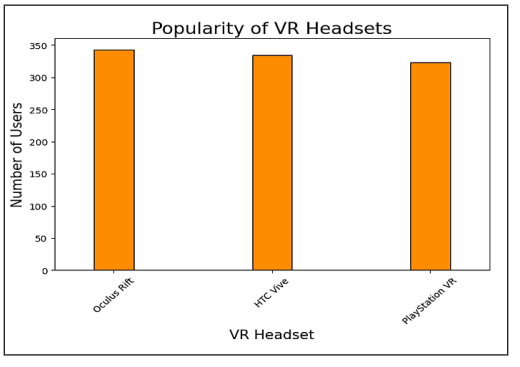

Figure 10. The number of users for each VR headset

Gender Distribution Analysis

Table 8 and Figure 11 present the dataset, including information on the gender of users who engaged with VR. Of the total users, the majority are males, constituting about 65% of the sample, while females are about 35%. This means that the gender distribution of users in VR is imbalanced, with male users more dominant than female users by a margin of 1.8:1. Such a disparity could be attributed to several factors, including differences in interests in technology, games, or other immersive experiences. Knowledge of this distribution is essential for VR developers and marketers who want to design content that is appealing to minorities and targets them effectively. For instance, developing VR experiences that target specific niches might attract more female users and help reduce the gender gap. Furthermore, this gender perspective might influence headset design, interface interactivity, and content selection, making VR technology more appealing to a wider public. In sum, the results presented shed light on the potential to improve gender representation in VR and make it more gender-balanced.

Table 8
The count of users by gender

S. No.	Number of Users	Gender
1	348	Others
2	330	Male
3	326	Female

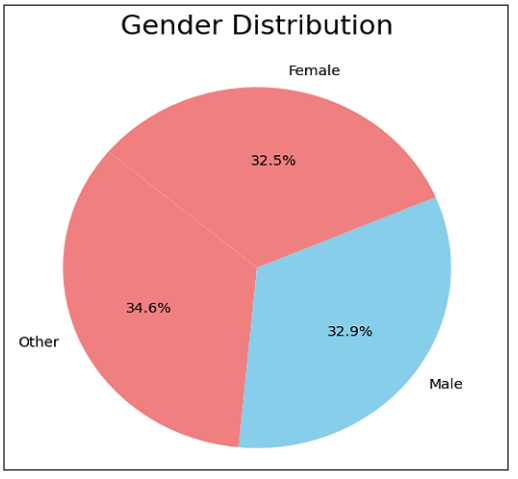

Figure 11. The count of users by gender

Table 9
Classification session lengths into ranges and their individual frequencies

S. No.	Duration Range	Frequency
1	(27.987, 31.456]	119
2	(48.978, 54.476]	112
3	(11.516, 17.003]	106
4	(38.927, 43.502]	101
5	(31.498, 38.893]	103
6	(21.501, 25.936]	98
7	(5.927, 11.423]	97
8	(44.493, 48.738]	94
9	(55.593, 59.963]	90
10	(16.002, 22.522]	87

Session Duration Distribution

Table 9 and Figure 12 present the session durations of VR experiences, indicating that the distribution of user time in VR differs significantly. The data was split into 10 equal-duration categories. A significant number of users, especially in the short-session category (less than 10 minutes), indicated that their use of the site was brief, exploratory, or casual. The most frequent range, however, is between 20 and 30 minutes, suggesting a sweet spot where users feel comfortable and

engaged before fatigue or other factors set in. Longer sessions, extending beyond 50 minutes, were relatively rare, representing only a small percentage of users. This could be attributed to motion sickness, hardware discomfort, or a natural tendency among users to limit their VR exposure in a single sitting. Notably, mid-range durations (30–40 minutes) still saw significant activity, reflecting deeper engagement with content such as games or simulations. These insights suggest that VR developers might consider optimising experiences for the 20–30-minute range to align with common user behaviour. Additionally, improving comfort and content for longer durations could help capture the smaller but valuable segment of extended-session users.

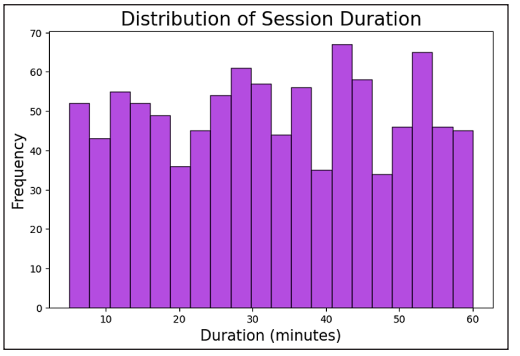

Figure 12. Classification session lengths into ranges

Session Duration by VR Headset Analysis

Table 10 and Figure 13 show that session durations vary significantly across VR headsets. Users of the HTC Vive had an average session duration of 34.7 minutes, with a standard deviation of 16.4 minutes, indicating a moderately variable range of session lengths. The shortest session observed was 6.0 minutes, while the longest reached 68.3 minutes. The median session duration was 35.6 minutes, suggesting that typical users spend approximately this amount of time in VR. For the Oculus Rift, the average session duration was slightly lower, at 34.1 minutes, with a standard deviation of 16.9 minutes, showing a similar range of session diversity. Sessions ranged from 6.5 minutes to 65.8 minutes, with a median duration of 31.0 minutes. Lastly, users of the PlayStation VR had the shortest average session duration, at 29.7 minutes, with a standard deviation of 16.8 minutes. Sessions ranged from 6.1 minutes to 60.1 minutes, with a median duration of 29.7 minutes. This comparison shows that HTC Vive users tend to engage in longer VR sessions, while PlayStation VR users tend to have shorter sessions on average.

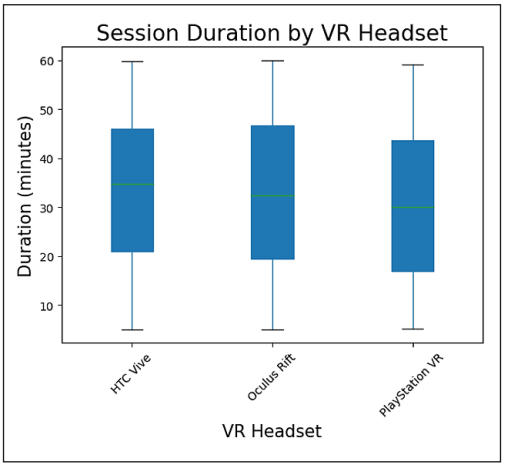

Figure 13. Durations for each VR headset

Table 10
Statistics (mean, median, quartiles) of session durations for each VR headset

S. No.	VR Headset	count	mean	std	min	25%	50%	75%	max
1	HTC Vive	335.0	34.78623 97724418 54	16.42787 66789976 89	6.003567 68789890 6	22.07534 56963435 67	35.65768 62334577 89	47.35789 90227889 35	60.88746 67878990 91
2	Oculus Rift	343.0	34.12249 75398546 89	16.96542 56892684 57	6.509987 52457886 7	17.49992 87567799 78	33.48966 46587882 56	47.34787 89646721 94	60.75664 53367899 92
3	PlayStation VR	323.0	29.78755 34013789 55	16.84567 99900365 90	6.157468 88900787 8	15.78843 29075799 53	29.78422 45768907 65	44.73678 78934328 76	60.18442 46678999 01

Motion Sickness vs Immersion Level Correlation Analysis

Table 11 and Figure 14 illustrate the correlation between motion sickness and immersion level, providing insights into their relationship. The correlation coefficient between motion sickness and immersion level is calculated as -0.12, indicating a weak negative correlation. This suggests that as motion sickness slightly increases, immersion levels may tend to decrease, though the effect is minimal. Further analysis of the correlation matrix reveals a self-correlation of 1.0 for both motion sickness and immersion level, as expected, since they are perfectly correlated with themselves. However, the cross-correlation value indicates that the relationship between these two variables is not strongly linear, suggesting that other factors may influence immersion levels in VR experiences. This weak negative correlation provides a basis for exploring whether reducing motion sickness symptoms could enhance user immersion, thereby informing future design improvements in VR applications and hardware.

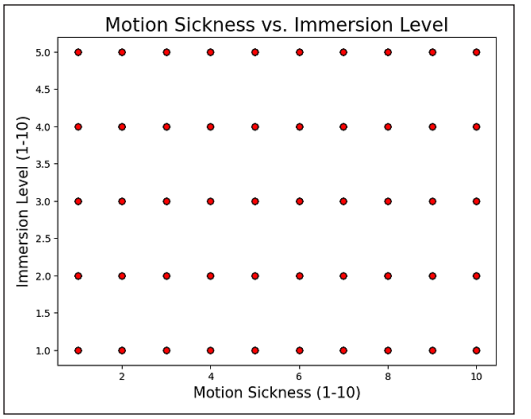

Figure 14. Correlations between motion sickness and immersion levels

Table 11
Correlations between motion sickness and immersion levels

S. No.	Metric 1	Metric 2	Correlation
1	Motion Sickness	Motion Sickness	1.0000000
2	Motion Sickness	Immersion Level	-0.038766778099755
3	Immersion Level	Motion Sickness	-0.038766778099755
4	Immersion Level	Immersion Level	1.00000000

Motion Sickness by VR Headset Analysis

Table 12 and Figure 15 show that the analysis of motion sickness levels across different VR headsets reveals interesting insights. On average, PlayStation VR users reported the highest motion sickness score of 5.73, with a standard deviation of 2.75. This suggests slightly greater variability in user experiences compared to other headsets. In contrast, HTC Vive users reported an average motion sickness score of 5.48, while Oculus Rift users had the lowest average score of 5.38, both with comparable variability (standard deviations of 2.96 and 2.88, respectively). The minimum motion sickness level was 1 across all headsets, indicating that some users experienced no symptoms. The maximum score of 10 was also consistent across headsets, showing that all devices caused severe motion sickness for a subset of users. Median scores indicate that the typical experience involved moderate symptoms, with medians ranging from 5 to 6 across devices. This data highlights that motion sickness is a significant consideration for all VR devices, though variations exist between headsets. PlayStation VR may warrant further investigation due to its slightly higher average motion sickness.

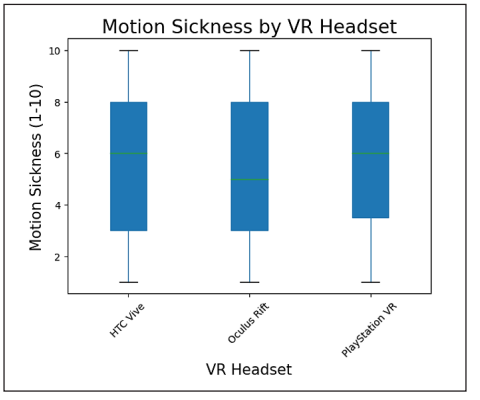

Figure 15. Descriptive statistics of motion sickness levels for each VR headset

Table 12
Descriptive statistics of motion sickness levels for each VR headset

S. No.	VR Headset	count	mean	std	min	25%	50%	75%	max
1	HTC Vive	335.0	5.476899 0456578 27	2.945678 7985434 77	1.0	3.0	6.0	8.0	10.0

Table 12 (*continued*)

S. No.	VR Headset	count	mean	std	min	25%	50%	75%	max
2	Oculus Rift	334.0	5.378752 1986645 78	2.856758 9464657 89	1.0	3.0	5.0	8.0	10.0
3	PlayStation VR	324.0	5.772389 7664323 79	2.746932 6789975 34	1.0	3.0	6.0	8.0	10.0

Ablation Study

The proposed model's modules each perform an important role. In this section, we conduct a series of ablation studies on cybersickness detection to compare the proposed MLT-DNN with current models, including 3D-CNN, SVM+TDA, and LSTM-Attention. To study performance development and validate our proposed MLT-DNN, new features derived from the model are gradually incorporated.

Table 13 and Figure 16 present an ablation study on the accuracy of various model configurations for cybersickness detection. The baseline model achieves 87.56% accuracy, and using only SOBI achieves 80.55%. The MTL-DNN configuration improves accuracy to 94.55%. Nevertheless, the accuracy of the Proposed Framework, which combines SOBI and MTL-DNN, is the highest at 97.16%, demonstrating that integrating such advanced signal pre-processing with multitask learning is beneficial. These outcomes indicate that the suggested framework increases the performance of cybersickness detection.

Table 13
Ablation study for accuracy analysis

Model Configuration	Accuracy
Baseline	87.56
SOBI Only	80.55
MTL-DNN Only	94.55
Proposed Framework	97.16

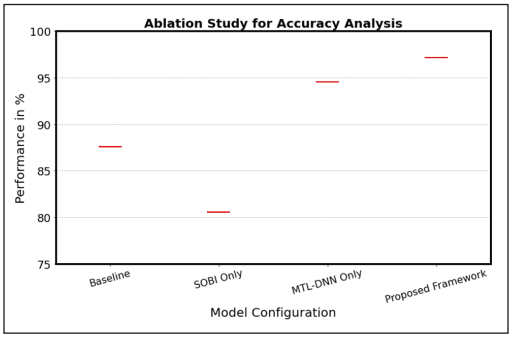

Figure 16. Ablation study for accuracy analysis

Table 14 and Figure 17 compare the accuracy of the proposed method with other state-of-the-art methods for physiological data-based assessment. The authors of Garcia-Agundez et al. (2019) achieved an accuracy of 82% using the SVM, KNN, and NN algorithms on ECG, EOG, EDA, and RESP signals. Pane et al. (2018) achieved 88.9% accuracy using EEG

data with SVM and CNN. Kim et al. (2019) improved the accuracy to 90.4% using a CNN-RNN architecture with video and EEG signals. Yalcin et al. (2024) achieved 91.7% accuracy using a Bidirectional LSTM and a CNN with multimodal physiological signals, including ECG, ACC, EDA, BVP, and TEMP. Such progression is attributed to the enhanced efficiency of the complex neural network architecture and multi-modal data fusion in enhancing accuracy.

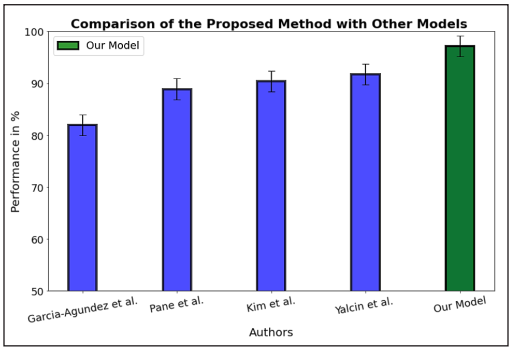

Figure 17. Comparison of the proposed method with the state-of-the-art methods for accuracy analysis

Table 14
Comparison of the proposed method with the state-of-the-art methods for accuracy analysis

Author's	Setup	Physio.Data	Methods	Accuracy
Garcia-Agundez et al., 2019	HMD, Electrode-based	ECG, EOG, EDA, RESP	SVM, KNN, NN	82
Pane et al., 2018	EEGSetup	EEG	SVM, CNN	88.9
Kim et al., 2019	EEGSetup	Video, EEG	CNN-RNN	90.4
Yalcin et al., 2024	HMD,PolarH10, Empatica	ECG, ACC, EDA, BVP, TEMP	Bid-LSTM, CNN	91.7
Our Model	128 GB memory, Intel i9-10900X CPU, and Nvidia RTX 3090 GPU	-	MLT-DNN	97.16

Limitations & Challenges

The application of deep learning and signal processing methods, including MTL-DNN and SOBI, in cybersickness detection has some important limitations and challenges. However, there are some drawbacks to the proposed MTL-DNN model: its high computational complexity may limit its real-time application on low-power devices. It also suggests that the assumption of signal independence, on which the method is based, may not be as advantageous for SOBI when noise levels are high and correlated or overlapping. Furthermore, for deep learning models, acquiring a large, high-quality EEG dataset is challenging because data collection in VR environments can be costly and time-consuming. The nature of physiological individual differences makes it very hard to apply the model across users, hence the need for flexibility in the approaches used for different users. These difficulties imply that more work is needed to extend the system's size and robustness, and to understand how to personalise it.

CONCLUSION

In conclusion, the effectiveness of combining advanced deep learning techniques with signal processing methods for the real-time detection of cybersickness in VR environments is demonstrated. By integrating an MTL-DNN with SOBI, the proposed framework achieves superior accuracy and robustness compared to traditional approaches. SOBI effectively pre-processes EEG signals by reducing artefacts and isolating meaningful independent components, while MTL-DNN leverages multitask learning to simultaneously predict cybersickness severity and related physiological states. Validated on benchmark EEG datasets, the framework shows enhanced performance in both detection accuracy and computational efficiency, offering a scalable solution for real-time monitoring. This synergy between deep learning and signal processing sets a new standard for objective detection of cybersickness, paving the way for improved user experiences in human-computer interaction.

FUTURE WORK

Future work will involve applying this framework to multimodal data, including eye tracking, heart rate, and motion sensors, to provide a more accurate estimate of cybersickness. Moreover, investigating an adaptive learning approach to identify cybersickness based on the user's EEG patterns and VR scenarios will expand the system's applicability. Adapting this framework with actual VR applications will also be a step towards designing user-oriented, realistic environments.

ACKNOWLEDGEMENT

Author Contributions: All authors contributed equally, and all authors read and approved the final version of the paper.

REFERENCES

Ahir, K., Govani, K., Gajera, R., & Shah, M. (2020). Application on virtual reality for enhanced education learning, military training and sports [Retracted article]. *Augmented Human Research, 5*, Article 7. https://doi.org/10.1007/s41133-019-0025-2

Alam, M. N., Ibrahimy, M. I., & Motakabber, S. M. A. (2021). Feature extraction of EEG signal by power spectral density for motor imagery based BCI. In *2021 8th International Conference on Computer and Communication Engineering (ICCCE)* (pp. 234-237). IEEE. https://doi.org/10.1109/iccce50029.2021.9467141

Caserman, P., Garcia-Agundez, A., Gámez Zerban, A., & Göbel, S. (2021). Cybersickness in current-generation virtual reality head-mounted displays: Systematic review and outlook. *Virtual Reality, 25*(4), 1153-1170. https://doi.org/10.1007/s10055-021-00513-6

Chang, C.-H., Lin, J., Chang, J.-W., Huang, Y.-S., Lai, M.-H., & Chang, Y.-J. (2024). Hybrid deep neural networks with multi-tasking for rice yield prediction using remote sensing data. *Agriculture, 14*(4), Article 513. https://doi.org/10.3390/agriculture14040513

Chang, E., Billinghurst, M., & Yoo, B. (2023). Brain activity during cybersickness: A scoping review. *Virtual Reality, 27*(3), 2073-2097. https://doi.org/10.1007/s10055-023-00795-y

Garcia-Agundez, A., Reuter, C., Becker, H., Konrad, R., Caserman, P., Miede, A., & Göbel, S. (2019). Development of a classifier to determine factors causing cybersickness in virtual reality environments. *Games for Health Journal, 8*(6), 439-444. https://doi.org/10.1089/g4h.2019.0045

Hadadi, A., Guillet, C., Chardonnet, J.-R., Langovoy, M., Wang, Y., & Ovtcharova, J. (2022). Prediction of cybersickness in virtual environments using topological data analysis and machine learning. *Frontiers in Virtual Reality, 3*, Article 973236. https://doi.org/10.3389/frvir.2022.973236

Heo, J., & Yoon, G. (2020). EEG studies on physical discomforts induced by virtual reality gaming. *Journal of Electrical Engineering & Technology, 15*(3), 1323-1329. https://doi.org/10.1007/s42835-020-00373-1

Joshi, A. (2023). *Virtual reality experiences* [Data set]. Kaggle. https://doi.org/10.34740/KAGGLE/DSV/5716193

Kim, J., Kim, W., Oh, H., Lee, S., & Lee, S. (2019). A deep cybersickness predictor based on brain signal analysis for virtual reality contents. In *2019 IEEE/CVF International Conference on Computer Vision (ICCV)* (pp. 10580-10589). IEEE. https://doi.org/10.1109/iccv.2019.01068

Kourtesis, P., Papadopoulou, A., & Roussos, P. (2024). Cybersickness in virtual reality: The role of individual differences, its effects on cognitive functions and motor skills, and intensity differences during and after immersion. *Virtual Worlds, 3*(1), 62-93. https://doi.org/10.3390/virtualworlds3010004

Krokos, E., & Varshney, A. (2022). Quantifying VR cybersickness using EEG. *Virtual Reality, 26*(1), 77-89. https://doi.org/10.1007/s10055-021-00517-2

Lee, T. M., Yoon, J.-C., & Lee, I.-K. (2019). Motion sickness prediction in stereoscopic videos using 3D convolutional neural networks. *IEEE Transactions on Visualization and Computer Graphics, 25*(5), 1919-1927. https://doi.org/10.1109/tvcg.2019.2899186

Liu, X., Wang, H., Huang, M., & Yang, W. (2019). An improved second-order blind identification (SOBI) signal de-noising method for dynamic deflection measurements of bridges using ground-based synthetic aperture radar (GBSAR). *Applied Sciences, 9*(17), Article 3561. https://doi.org/10.3390/app9173561

Martin, N., Mathieu, N., Pallamin, N., Ragot, M., & Diverrez, J.-M. (2020). Virtual reality sickness detection: An approach based on physiological signals and machine learning. In *2020 IEEE International Symposium on Mixed and Augmented Reality (ISMAR)* (pp. 387-399). IEEE. https://doi.org/10.1109/ismar50242.2020.00065

Martirosov, S., Bureš, M., & Zítka, T. (2022). Cyber sickness in low-immersive, semi-immersive, and fully immersive virtual reality. *Virtual Reality, 26*(1), 15-32. https://doi.org/10.1007/s10055-021-00507-4

Pane, E. S., Khoirunnisaa, A. Z., Wibawa, A. D., & Purnomo, M. H. (2018). Identifying severity level of cybersickness from EEG signals using CN2 rule induction algorithm. In *2018 International Conference on Intelligent Informatics and Biomedical Sciences (ICIIBMS)* (Vol. 3, pp. 170-176). IEEE. https://doi.org/10.1109/iciibms.2018.8549968

Papaefthymiou, S., Giannakopoulos, A., Roussos, P., & Kourtesis, P. (2024). Mitigating cybersickness in virtual reality: Impact of eye–hand coordination tasks, immersion, and gaming skills. *Virtual Worlds, 3*(4), 506-535. https://doi.org/10.3390/virtualworlds3040027

Porcino, T., Trevisan, D., & Clua, E. (2020). Minimizing cybersickness in head-mounted display systems: Causes and strategies review. In *2020 22nd Symposium on Virtual and Augmented Reality (SVR)* (pp. 154-163). IEEE. https://doi.org/10.1109/svr51698.2020.00035

Qu, C., Che, X., Ma, S., & Zhu, S. (2022). Bio-physiological-signals-based VR cybersickness detection. *CCF Transactions on Pervasive Computing and Interaction, 4*(3), 268-284. https://doi.org/10.1007/s42486-022-00103-8

Sameri, J., Coenegracht, H., Van Damme, S., De Turck, F., & Torres Vega, M. (2024). Physiology-driven cybersickness detection in virtual reality: A machine learning and explainable AI approach. *Virtual Reality, 28*(4), Article 174. https://doi.org/10.1007/s10055-024-01067-z

Teixeira, J., & Palmisano, S. (2021). Effects of dynamic field-of-view restriction on cybersickness and presence in HMD-based virtual reality. *Virtual Reality, 25*(2), 433-445. https://doi.org/10.1007/s10055-020-00466-2

Yalcin, M., Halbig, A., Fischbach, M., & Latoschik, M. E. (2024). Automatic cybersickness detection by deep learning of augmented physiological data from off-the-shelf consumer-grade sensors. *Frontiers in Virtual Reality, 5*, Article 1364207. https://doi.org/10.3389/frvir.2024.1364207

Yang, A. H. X., Kasabov, N., & Cakmak, Y. O. (2022). Machine learning methods for the study of cybersickness: A systematic review. *Brain Informatics, 9*(1), Article 24. https://doi.org/10.1186/s40708-022-00172-6

Zaidi, S. F. M., Shafiabady, N., & Beilby, J. (2023). Identifying presence of cybersickness symptoms using AI-based predictive learning algorithms. *Virtual Reality, 27*(4), 3613-3620. https://doi.org/10.1007/s10055-023-00813-z